Experimental Mechanics manuscript No.
(will be inserted by the editor)

Measurement of the distribution of residual stresses in layered thick-walled GFRP pipes

H.W. Carpenter · R.G. Reid · R. Paskaramoorthy

12 June 2014

Abstract The objective of this study is to measure the axial, circumferential, shear and radial residual stress distributions in three thick-walled glass fibre reinforced plastic (GFRP) filament-wound pipes, two of which are layered. The measurement of residual stresses was carried out using a recently published layer removal method which overcomes the limitations of previous techniques and can be applied to layered anisotropic pipes of any wall thickness. Layers of approximately 0.3 mm thickness were incrementally ground from the outer surface of the pipes. The resulting strains were measured on the inner surfaces. A least-squares polynomial was fitted to each measured data set, and used to calculate the corresponding stress distributions. All of the resulting axial, hoop and shear stress distributions adhere to the requirement of self-equilibrium and the radial stress distributions all vanish to zero at the inner and outer surfaces. The radial stresses of the layered pipes showed a

H.W. Carpenter · R.G. Reid (✉) · R. Paskaramoorthy

DST/NRF Centre of Excellence in Strong Materials and RP/Composites Facility

School of Mechanical, Industrial and Aeronautical Engineering

University of the Witwatersrand, Johannesburg

Private Bag 3, Wits, 2050, South Africa

E-mail: robert.reid@wits.ac.za

tendency to have two peaks, one for each layer, a consequence of the two-stage manufacturing process of these pipes. The measured axial and hoop stresses of all three pipes were similar at the inner surfaces despite significant differences in the stiffnesses in the principal directions arising from different wind angles.

Keywords Residual stress · Layer removal · Filament winding

1 Introduction

GFRP pipes are used in many industries due to their excellent strength to weight ratio and good corrosion resistance. In addition, the smooth surface finish on the inner wall of GFRP pipes allows the frictional losses associated with fluid flow to be minimised. Thick walls are required where high operating pressures exist and this promotes the development of residual stresses. These stresses arise from a number of factors including the cure shrinkage of the resin system, differences in the coefficients of thermal expansion of the fibre and resin system and changes in the stiffnesses and coefficients of thermal expansion arising from variations in fibre direction. Although the residual stresses are typically low, the large safety factors used in the design of thick-walled GFRP pipes results in mechanical stresses that are comparable. Neglecting residual stresses in such cases completely misrepresents the state of stress. The residual stresses that develop in GFRP pipes are typically tensile on the inner surface. Stresses resulting from mechanical loading are also tensile and so the combination of these tensile stresses makes the pipes susceptible to environmentally assisted cracking, which tends to negate the important advantage of corrosion resistance. In addition, in very thick-walled pipes the radial residual stresses can become sufficiently large to cause cracking [1] that leads to delamination. It thus becomes important to be able to measure the residual stresses within thick-walled GFRP pipes.

The most common techniques used in determining residual stresses include the layer removal method [2,3], crack compliance or slitting method [4–7], contour method [8,9], hole drilling method [10,11] and Sachs' method [12,13]. In cylindrical composite sections, a slitting type approach is most frequently used to obtain the residual stress. An estimate of the circumferential residual stress within a cylindrical part is obtained by cutting a slit through the thickness down the length of the cylinder to release the inherent bending moment. Kim and Lee [14] utilised this method together with the curved-beam theory to obtain the residual hoop stresses in thick-walled carbon fibre cylinders. Seif et al. [15,16] determined the residual stress distribution in thin-walled composite cylinders using this method together with optical displacement measurement. The crack compliance method is an extension to this approach. It allows the through thickness residual stress state to be determined through incremental slitting. Akbari et al. [17] utilised the crack compliance method, with pulse functions and Thikhonov regularization to obtain the hoop stress distribution in a layered carbon fibre ring.

Although the slitting technique is most frequently used to determine only the residual stress distribution normal to the slit direction, it has been shown [4] that the axisymmetric residual stresses in an isotropic pipe can be determined through measuring only the variation in circumferential strain as a slit is extended in the radial direction of a pipe in both plane strain and plane stress. These results can be combined to estimate the axial, radial and hoop residual stresses. The method could be extended to laminated composite pipes by using the finite element method to determine the compliances of the two pipe configurations. This procedure can be time consuming, however, and would need to be repeated for every change in pipe configuration. The method of Sachs [12] has a different approach. It relies on the boring out of the inner surface, or removal of outer surface layers of a pipe, and can thus be considered a layer removal method. The method was originally developed for

isotropic cylindrical bodies and has been widely used in this context [13,18,19]. It has also been extended for application on composite pipes. Chen et al. [20] proposed a variant of the technique that utilises an inherent strain analysis to determine the residual stress distribution in layered isotropic pipes. Olson and Bert [21] modified Sachs' method so that the residual stresses in cylindrically orthotropic bars and tubes could be determined. Voyiadjis et al. [22] presented a similar method for determining the residual stresses in cylindrically orthotropic materials. Voyiadjis et al. [23] later presented an extension of this work to include layered orthotropic materials. None of these methods can be used to determine the residual stresses in very thick-walled orthotropic pipes and none can do so in anistropic pipes [24]. Carpenter et al. [24] recently proposed a method that addresses these issues and extends the previous capabilities to allow the residual stresses in layered anisotropic pipes of any wall thickness to be determined. This tool makes it possible to accurately measure the residual stresses in thick-walled filament wound pipes. The objective of the present work is to measure the residual stresses in three different filament wound pipes and discuss how these are influenced by the manufacturing parameters.

2 Theory

The derivation of this method is based on the exact elasticity solution for a laminated pipe presented in the textbook of Herakovich [25]. The method is fully described in the paper of Carpenter et al. [24] and so only details germane to the problem at hand are presented here. The term "ply" throughout the following derivation is reserved for a single lamina within the pipe laminate, whereas the term "layer" refers to the material that has been removed in the layer removal process. Measurement of the residual stresses through the thickness of a ply requires the removal of a number of layers. As each layer is removed, the elastic

response of the remaining pipe section is measured. The analytical technique that allows the variation in strains measured in the remaining pipe section to be related to the original stress distribution assumes that the pipe is axisymmetric, infinitely long and uniformly loaded along its length [25]. The mechanical loads, F_x and T_x, required to exist at the ends of the pipe are found by integrating the axial stresses and the moment of the shear stresses over the wall thickness, respectively. The pressure loads P_O and P_I are uniformly distributed over the inner and outer surfaces of the pipe.

The laminated pipe under consideration is illustrated in Fig. 1. For a fibre angle ϕ mea-

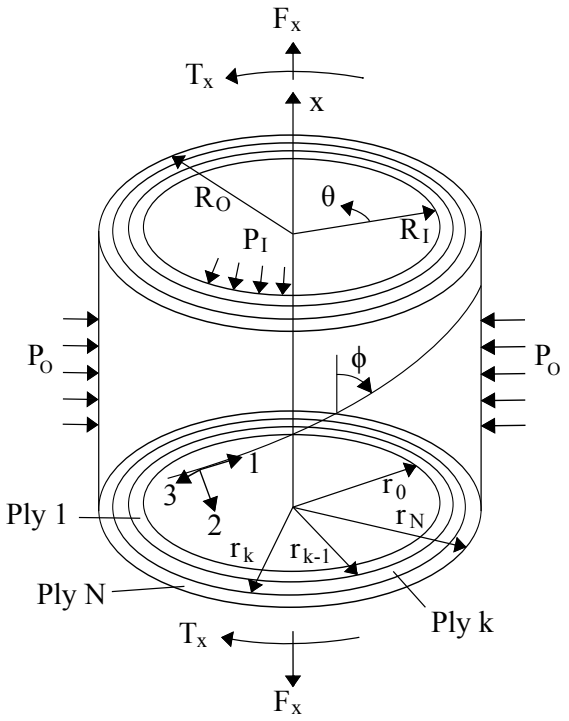

Fig. 1 Laminated composite pipe

sured relative to the axial direction of the pipe, the elastic constitutive equations in the cylindrical coordinate system (r, θ, x) [25] are reduced to

$$\begin{bmatrix} \sigma_x \\ \sigma_\theta \\ \sigma_r \\ \tau_{x\theta} \end{bmatrix} = \begin{bmatrix} \bar{C}_{11} & \bar{C}_{12} & \bar{C}_{13} & \bar{C}_{16} \\ \bar{C}_{12} & \bar{C}_{22} & \bar{C}_{23} & \bar{C}_{26} \\ \bar{C}_{13} & \bar{C}_{23} & \bar{C}_{33} & \bar{C}_{36} \\ \bar{C}_{16} & \bar{C}_{26} & \bar{C}_{36} & \bar{C}_{66} \end{bmatrix} \begin{bmatrix} \varepsilon_x \\ \varepsilon_\theta \\ \varepsilon_r \\ \gamma_{x\theta} \end{bmatrix} \tag{1}$$

since the interlaminar shear stresses $\tau_{\theta r}$ and τ_{xr} are zero at points some distance from the ends of the pipe [25]. The radial displacement [25], w, is

$$w^k(r) = A_1^k r^{\lambda^k} + A_2^k r^{-\lambda^k} + \Gamma^k \varepsilon_x^0 r + \Omega^k \gamma^0 r^2 \tag{2}$$

where ε_x^0, γ^0, A_1^k and A_2^k are constants determined by the specified boundary and loading conditions. The terms λ^k, Γ^k and Ω^k are constant terms dependent on the material properties of the k^{th} ply [25]:

$$\lambda^k = \sqrt{\frac{\bar{C}_{22}^k}{\bar{C}_{33}^k}} \tag{3}$$

$$\Gamma^k = \frac{\bar{C}_{12}^k - \bar{C}_{13}^k}{\bar{C}_{33}^k - \bar{C}_{22}^k} \tag{4}$$

$$\Omega^k = \frac{\bar{C}_{26}^k - 2\bar{C}_{36}^k}{4\bar{C}_{33}^k - \bar{C}_{22}^k} \tag{5}$$

Individual ply strains, ε_x^k, ε_θ^k and $\gamma_{x\theta}^k$, at the radial position r for the k^{th} ply can be written [25] as

$$\varepsilon_x^k = \varepsilon_x^0 \tag{6}$$

$$\varepsilon_\theta^k = A_1^k r^{(\lambda^k - 1)} + A_2^k r^{(-\lambda^k - 1)} + \Gamma^k \varepsilon_x^0 + \Omega^k \gamma^0 r \tag{7}$$

$$\gamma_{x\theta}^k = \gamma^0 r \tag{8}$$

The stresses in the k^{th} ply, at the radial position r, are determined using Eqs. (9) to (12) [25]:

$$\begin{aligned}\sigma_x^k = &\left[\bar{C}_{11}^k + \left(\bar{C}_{13}^k + \bar{C}_{12}^k\right)\Gamma^k\right]\varepsilon_x^0 + \left[\left(\bar{C}_{12}^k + 2\bar{C}_{13}^k\right)\Omega^k + \bar{C}_{16}^k\right]\gamma^0 r \\ &+ \left[\bar{C}_{12}^k + \lambda^k \bar{C}_{13}^k\right] A_1^k r^{(\lambda^k - 1)} + \left[\bar{C}_{12}^k - \lambda^k \bar{C}_{13}^k\right] A_2^k r^{(-\lambda^k - 1)}\end{aligned} \tag{9}$$

$$\begin{aligned}\sigma_\theta^k = &\left[\bar{C}_{12}^k + \left(\bar{C}_{22}^k + \bar{C}_{23}^k\right)\Gamma^k\right]\varepsilon_x^0 + \left[\left(\bar{C}_{22}^k + 2\bar{C}_{23}^k\right)\Omega^k + \bar{C}_{26}^k\right]\gamma^0 r \\ &+ \left[\bar{C}_{22}^k + \lambda^k \bar{C}_{23}^k\right] A_1^k r^{(\lambda^k - 1)} + \left[\bar{C}_{22}^k - \lambda^k \bar{C}_{23}^k\right] A_2^k r^{(-\lambda^k - 1)}\end{aligned} \tag{10}$$

$$\begin{aligned}\sigma_r^k = &\left[\bar{C}_{13}^k + \left(\bar{C}_{23}^k + \bar{C}_{33}^k\right)\Gamma^k\right]\varepsilon_x^0 + \left[\left(\bar{C}_{23}^k + 2\bar{C}_{33}^k\right)\Omega^k + \bar{C}_{36}^k\right]\gamma^0 r \\ &+ \left[\bar{C}_{23}^k + \lambda^k \bar{C}_{33}^k\right] A_1^k r^{(\lambda^k - 1)} + \left[\bar{C}_{23}^k - \lambda^k \bar{C}_{33}^k\right] A_2^k r^{(-\lambda^k - 1)}\end{aligned} \tag{11}$$

$$\begin{aligned}\tau_{x\theta}^k = &\left[\bar{C}_{16}^k + \left(\bar{C}_{26}^k + \bar{C}_{36}^k\right)\Gamma^k\right]\varepsilon_x^0 + \left[\bar{C}_{66}^k + \left(\bar{C}_{26}^k + 2\bar{C}_{36}^k\right)\Omega^k\right]\gamma^0 r \\ &+ \left[\bar{C}_{26}^k + \lambda^k \bar{C}_{36}^k\right] A_1^k r^{(\lambda^k - 1)} + \left[\bar{C}_{26}^k - \lambda^k \bar{C}_{36}^k\right] A_2^k r^{(-\lambda^k - 1)}\end{aligned} \tag{12}$$

For perfectly bonded plies, all displacements must be continuous across the interface between plies. This requirement applies also to the radial stress, σ_r, and the interlaminar shear stresses, τ_{xr} and $\tau_{\theta r}$. The latter stresses vanish, however, some distance from the end of the pipe. The radial stress at the inner and outer walls of the pipe is exactly equal and opposite to the pressure applied on the respective surfaces. These requirements are used to obtain the constants ε_x^0 and γ^0 and the ply constants A_1^k and A_2^k [25].

$$\varepsilon_x^{0^k} = \varepsilon_x^0 \quad (k = 1, \ldots, N) \tag{13}$$

$$\gamma^{0^k} = \gamma^0 \quad (k = 1, \ldots, N) \tag{14}$$

$$w^k = w^{k+1} \quad (\text{Interface at } r_k \; k = 1, \ldots, N-1) \tag{15}$$

$$\sigma_r^k = \sigma_r^{k+1} \quad (\text{Interface at } r_k \; k = 1, \ldots, N-1) \tag{16}$$

$$\sigma_r(R_I) = -P_I \tag{17}$$

$$\sigma_r(R_O) = -P_O \tag{18}$$

In the above, P is the pressure and the subscripts I and O refer to the inner and outer surfaces, respectively.

Obtaining residual stresses

The residual stress distribution is determined by progressively releasing stress through the removal of material, and measuring the associated changes in strain elsewhere in the pipe. It is assumed in this work that the removal of material progresses inwards from the outside of the pipe and that the strain is measured on the inner surface. Removal of material in the reverse direction can, however, easily be accommodated. The assumption is made that the removal of a layer of material from the outer surface of the pipe causes a purely elastic mechanical response in the remaining pipe section. Strain gauge rosettes are required so that the axial strain, ε_x, hoop strain, ε_θ, and in-plane shear strain, $\gamma_{x\theta}$, responses can be determined. Since the constants ε_x^0 and γ^0 that arise in the response to the release of residual stress in the removed layer are invariant throughout the remaining wall thickness, $\varepsilon_x = \varepsilon_x^0$ and $\gamma_{x\theta} = \gamma^0 R_I$.

The depth of each layer removed is entirely independent of the thickness of each ply. The measured strains after the removal of m layers allow the calculation of the residual load that has been released. The load can be modelled as an axial force and torque applied to the remaining pipe of N plies, as well as an external pressure applied at the newly exposed outer surface. The requirement is that the application of these loads must result in the same strains that are measured after the removal of all m layers of material from the outside of the pipe.

Prior to the calculation of the loads applied to the remaining pipe thickness, the ply constants A_1^k and A_2^k are determined in this section. The number of plies remaining is equal to N which means that N constants A_1^k and N constants A_2^k must be determined, or $2(N)$ unknowns in total. This is done by utilising Eq. (11) where the radial stress at the inner surface of the pipe is always zero, and Eq. (7) where the measured strain is analytically expressed in relation to the required constants. Additionally, the $2(N-1)$ equilibrium conditions are si-

multaneously applied in the form of Eqs. (16) and (15) at each ply interface, which requires the use of Eqs. (11) and (2). In the case of the layered pipes in question, the number of plies is equal to two. The resulting equations for the case where $N = 2$ are given [24] by:

$$\begin{bmatrix} \beta^1 r_0^{(\lambda^1-1)} & \delta^1 r_0^{(-\lambda^1-1)} & 0 & 0 \\ r_0^{(\lambda^1-1)} & r_0^{(-\lambda^1-1)} & 0 & 0 \\ \beta^1 r_1^{(\lambda^1-1)} & \delta^1 r_1^{(-\lambda^1-1)} & -\beta^2 r_1^{(\lambda^2-1)} & -\delta^2 r_1^{(-\lambda^2-1)} \\ r_1^{\lambda^1} & r_1^{-\lambda^1} & -r_1^{\lambda^2} & -r_1^{-\lambda^2} \end{bmatrix} \begin{bmatrix} A_1^1 \\ A_2^1 \\ A_1^2 \\ A_2^2 \end{bmatrix} = \begin{bmatrix} -\eta^1 \varepsilon_x^0 - \kappa^1 \gamma^0 r_0 \\ \varepsilon_\theta^m - \Gamma^1 \varepsilon_x^0 - \Omega^1 \gamma^0 r_0 \\ -\eta^1 \varepsilon_x^0 - \kappa^1 \gamma^0 r_1 + \eta^2 \varepsilon_x^0 + \kappa^2 \gamma^0 r_1 \\ -\Gamma^1 \varepsilon_x^0 r_1 - \Omega^1 \gamma^0 r_1^2 + \Gamma^2 \varepsilon_x^0 r_1 + \Omega^2 \gamma^0 r_1^2 \end{bmatrix} \tag{19}$$

where

$$\beta^k = \bar{C}_{23}^k + \lambda^k \bar{C}_{33}^k \tag{20}$$

$$\delta^k = \bar{C}_{23}^k - \lambda^k \bar{C}_{33}^k \tag{21}$$

$$\eta^k = \bar{C}_{13}^k + \left[\bar{C}_{23}^k + \bar{C}_{33}^k\right] \Gamma^k \tag{22}$$

$$\kappa^k = \left[\bar{C}_{23}^k + 2\bar{C}_{33}^k\right] \Omega^k + \bar{C}_{36}^k \tag{23}$$

Reverting to the general case, once the constants in the remaining pipe section are known, the internal stresses and the pressure applied to the outer surface can be found using Eqs. (9) to (12) while invoking Eq. (18). These stresses result from the removal of the outer m layers of pipe section and are modelled as externally applied loads acting in the remaining pipe thickness. The axial force, F_x, and torque, T_x, existing at the ends of the remaining pipe of N plies are shown in Eqs. (24) and (25), respectively.

$$\begin{aligned} F_x =& 2\pi \sum_{k=1}^{N} \Bigg[\left(\bar{C}_{11}^k + \left\{ \bar{C}_{13}^k + \bar{C}_{12}^k \right\} \Gamma^k \right) \varepsilon_x^0 \left(\frac{r_k^2 - r_{k-1}^2}{2} \right) \\ &+ \left(\bar{C}_{16}^k + \left\{ \bar{C}_{12}^k + 2\bar{C}_{13}^k \right\} \Omega^k \right) \gamma^0 \left(\frac{r_k^3 - r_{k-1}^3}{3} \right) \\ &+ \frac{\left(\bar{C}_{12}^k + \lambda^k \bar{C}_{13}^k \right)}{\lambda^k + 1} A_1^k \left(r_k^{(\lambda^k+1)} - r_{k-1}^{(\lambda^k+1)} \right) \\ &+ \frac{\left(\bar{C}_{12}^k - \lambda^k \bar{C}_{13}^k \right)}{-\lambda^k + 1} A_2^k \left(r_k^{(-\lambda^k+1)} - r_{k-1}^{(-\lambda^k+1)} \right) \Bigg] \end{aligned} \tag{24}$$

$$\begin{aligned} T_x =& 2\pi \sum_{k=1}^{N} \Bigg[\left(\bar{C}_{16}^k + \left\{ \bar{C}_{26}^k + \bar{C}_{36}^k \right\} \Gamma^k \right) \varepsilon_x^0 \left(\frac{r_k^3 - r_{k-1}^3}{3} \right) \\ &+ \left(\bar{C}_{66}^k + \left\{ \bar{C}_{26}^k + 2\bar{C}_{36}^k \right\} \Omega^k \right) \gamma^0 \left(\frac{r_k^4 - r_{k-1}^4}{4} \right) \\ &+ \frac{\left(\bar{C}_{26}^k + \lambda^k \bar{C}_{36}^k \right)}{\lambda^k + 2} A_1^k \left(r_k^{(\lambda^k+2)} - r_{k-1}^{(\lambda^k+2)} \right) \\ &+ \frac{\left(\bar{C}_{26}^k - \lambda^k \bar{C}_{36}^k \right)}{-\lambda^k + 2} A_2^k \left(r_k^{(-\lambda^k+2)} - r_{k-1}^{(-\lambda^k+2)} \right) \Bigg] \end{aligned} \tag{25}$$

The loads released by each individual layer, $F_x^{\bar{m}}$ and $T_x^{\bar{m}}$, are found by subtracting the loads that exist after $m-1$ layers are removed from those that exist after m layers are removed.

$$F_x^{\bar{m}} = \begin{cases} F_x^m & (\text{for } m = 1) \\ F_x^m - F_x^{m-1} & (\text{for } m > 1) \end{cases} \tag{26}$$

$$T_x^{\bar{m}} = \begin{cases} T_x^m & (\text{for } m = 1) \\ T_x^m - T_x^{m-1} & (\text{for } m > 1) \end{cases} \tag{27}$$

The applied pressure, P_O^m, is found by using Eqs. (11) and (18). The resultant radial stress at the surface, after the removal of m layers, is the sum of the radial residual stress that existed prior to the removal of the outer layers and the calculated radial stress that arises due to the removal of these layers. The resultant radial stress at the outer surface of the remaining pipe must be zero, and so the residual radial stress is equal the the negative of the radial stress calculated using Eq. (11) and is thus exactly equal to the applied pressure P_O^m.

The stresses at the mid-radius of the newly removed layer m can be determined considering that the calculation of these stresses requires knowledge of the four constants A_1, A_2, ε_x^0 and γ^0 within this layer. These four unknowns are determined making use of the four boundary conditions arising from the application of the axial and torsional loads, $F_x^{\bar{m}}$ and $T_x^{\bar{m}}$, and the known radial residual stresses that were obtained for the inner and outer surfaces of this layer. If the removed layer contains an interface between two different materials, the appropriate boundary conditions of Eqs. (15) and (16) must also be included into the solution. Special mention must be made that it is assumed that the values of ε_x^0 and γ^0 are constant within the removed layer. Although these terms are constant when the pipe is mechanically loaded as prescribed in Fig. 1, the original residual stresses within the pipe were produced by processes that can be highly non-linear. As a consequence, it is improbable that the terms ε_x^0 and γ^0 are uniform within the pipe or the layer that is removed. The variation in the residual

stress that existed within each removed layer cannot therefore be found when considering only that individual layer. The thinner the layer that is removed, however, the more likely it is that the values of ε_x^0 and γ^0 can be assumed constant within that layer. Additionally, if the removed layers are thin enough, the average stress calculated at the mid radius is very similar to the residual stress that existed at the mid-radius of the layer. Thus the variation in the original residual stress is found by the combination of the stress results at the mid-radius of every removed layer.

Error analysis

The error in each of the axial, hoop, radial and shear stresses in the removed layer m can be expressed [26] as

$$e_{\sigma_i}^m = \sqrt{\left(\frac{\partial \sigma_i^m}{\partial \varepsilon_x^m} e_{\varepsilon_x}^m\right)^2 + \left(\frac{\partial \sigma_i^m}{\partial \varepsilon_\theta^m} e_{\varepsilon_\theta}^m\right)^2 + \left(\frac{\partial \sigma_i^m}{\partial \gamma_{x\theta}^m} e_{\gamma_{x\theta}}^m\right)^2} \tag{28}$$

where σ_i represents each of the stress components in layer m and $e_{\varepsilon_i}^m$ is the corresponding error. Should a polynomial be fitted to the data to represent the strain distribution, the error in strain is taken to be either the difference between the polynomial value and the measured strain, or the actual strain measurement uncertainty, whichever is the greater. This approach is the same as described by Prime and Hill [27] when employing the slitting method.

Since the stresses are not calculated directly from the measured strains, the partial derivative terms of Eq. (28) cannot be found in a straightforward way. Instead, the errors are estimated by considering the response of the stress components to the loads applied to each layer. In this case, the error in each stress component in layer m can be described as

$$e_{\sigma_i}^m = \sqrt{\left(\frac{\partial \sigma_i^m}{\partial F_x^{\tilde{m}}} e_{F_x}^m\right)^2 + \left(\frac{\partial \sigma_i^m}{\partial T_x^{\tilde{m}}} e_{T_x}^m\right)^2 + \left(\frac{\partial \sigma_i^m}{\partial P_i^m} e_{P_I}^m\right)^2 + \left(\frac{\partial \sigma_i^m}{\partial P_O^m} e_{P_O}^m\right)^2} \tag{29}$$

where $e_{F_x}^m$, $e_{T_x}^m$, $e_{P_I}^m$ and $e_{P_O}^m$ represent the errors in each of the loads applied to layer m. The error associated with each of the applied loads of Eq. (29) can be expressed as

$$e_{L_i}^m = \sqrt{\left(\frac{\partial L_i^{\tilde{m}}}{\partial \varepsilon_x^m} e_{\varepsilon_x}^m\right)^2 + \left(\frac{\partial L_i^{\tilde{m}}}{\partial \varepsilon_\theta^m} e_{\varepsilon_\theta}^m\right)^2 + \left(\frac{\partial L_i^{\tilde{m}}}{\partial \gamma_{x\theta}^m} e_{\gamma_{x\theta}}^m\right)^2} \tag{30}$$

where $L_i^{\tilde{m}}$ represents each of the loads applied to layer m, and $e_{\varepsilon_x}^m$, $e_{\varepsilon_\theta}^m$ and $e_{\gamma_{x\theta}}^m$ represent the error in each of the measured strain components. The partial derivative terms of Eq. (30) are estimated by finding each term separately. This is done numerically by varying the term in question, while holding the other measurement terms constant. It should be recognized that as a consequence of Eqs. (26) and (27), the error terms $e_{F_x}^m$ and $e_{T_x}^m$ depend on the errors associated with F_x and T_x after the removal of m and $m-1$ layers, and so

$$e_{F_x}^m = \sqrt{\left(\hat{e}_{F_x}^m\right)^2 + \left(\hat{e}_{F_x}^{m-1}\right)^2} \tag{31}$$

$$e_{T_x}^m = \sqrt{\left(\hat{e}_{T_x}^m\right)^2 + \left(\hat{e}_{T_x}^{m-1}\right)^2} \tag{32}$$

where $\hat{e}_{F_x}^m$, $\hat{e}_{T_x}^m$, $\hat{e}_{F_x}^{m-1}$ and $\hat{e}_{T_x}^{m-1}$ are the errors associated with the applied axial and torque loads after the removal of m and $m-1$ layers, respectively.

Once the errors in the loads applied to each layer m are estimated, the error in each stress component of Eq. (29) is estimated. This is done using an approach similar to that used to

find the errors in load. Each partial differential term of Eq. (29) is determined numerically by varying each term in turn while keeping the other terms fixed. Since no smoothing functions are used in determining the error bounds for each data point, the method assumes that all the noise around the strain curve are possible results of the stress distribution. The method is therefore quite conservative. Also, the magnitude of the error in stress within a removed layer depends heavily on the thickness of the layer itself. This is because the error in load is determined from the mechanical behaviour of the remaining pipe. For the same error in load, two layers of different thickness will result in different errors in stress. The thinner layer will produce larger errors because the error in load is distributed over a smaller surface area. There thus exists a trade off, in its current format, between, on the one hand, the number of data points needed to accurately define the residual stress distribution and also ensure that ε_x^0 and γ^0 can be assumed constant within each layer and, on the other hand, the error associated with the measurement itself.

3 Experiment

Test pieces

The experimental work was performed on three filament wound GFRP pipes manufactured by GRP Tubing (Pty) Ltd of South Africa. All three pipes had an inner diameter of 80 mm with a wall-thickness of 15 mm. This yields a thickness to inner diameter ratio (t/d_i) of 0.1875. The fibre used was E-glass and the epoxy resin system was Epikote L 1100 with the Epikure 294 curing agent. The fibre volume fraction was specified by the manufacturer to be in the range of 0.529 to 0.567. For the purposes of this work, the fibre volume fraction was taken as 0.548, the mean value within the specified range. Due to the impracticality of measuring the material properties of the curved laminate making up the wall thickness,

the material properties in the fibre coordinate system were estimated using micromechanics and are listed in Table 1. The fibre properties used in this analysis are well documented [25, 28] and the matrix properties were experimentally measured. The first of the pipes was wound entirely at the industry standard winding angle of $\pm 55°$. The cure cycle consisted of curing the pipe at room temperature for a period of 12 hours, followed by 2 hours at 60°C and then 8 hours at 80°C. Once cured, the pipe was ground to the desired thickness and then removed from the steel mandrel. The two remaining pipes were each made up of two different winding angles. These laminated pipes had an inner ply thickness of 5 mm and an outer ply thickness of 10 mm. The first of these pipes had an inner winding angle of $\pm 65°$ and outer winding angle of $\pm 47°$. The second was wound at $\pm 75°$ and $\pm 36°$. The laminated pipes were manufactured in two stages. The first stage consisted of winding the inner section and curing it in the same manner as the $\pm 55°$ pipe. The inner section was then ground to the desired thickness of 5 mm, after which the outer section was wound, and cured. After the final cure, the pipes were ground to the overall desired thickness of 15 mm and the mandrel was removed. The length of each pipe section used for experimental purposes was the subject of some investigation. It was necessary for each pipe section to be comparatively short so that the inner surface of the mid-length region could be properly accessed to accurately align the strain gauges and properly solder the lead wires. If the pipe was too short, however, far-field conditions would not be reached in the mid-length region of the pipe. To establish the required length, a finite element analysis was performed using axisymmetric models. The self-equilibriating thermal stresses that exist in pipes of varying lengths were compared to those in a pipe of infinite length which was modelled by imposing constant axial strain. It was found that the pipes needed to be about 220 mm in length for far-field conditions to exist. This length was too long, however, for practicality. Pipe sections of 120 mm in length were found to experience stresses within 5% of the far-field stresses. This

accuracy was considered acceptable for the purposes of this investigation and pipe sections of 120 mm length were consequently used. Three sets of strain gauge rosettes (orientated at 0°, 45° and 90° relative to the axial direction) were bonded to the inner surface at the mid-length of each test section, located circumferentially at 120° to one another, as seen in Fig. 2.

Table 1 Material properties

Longitudinal modulus, E_1 (MPa)	40887
Transverse modulus, $E_2 = E_3$ (MPa)	7905
Shear modulus, $G_{12} = G_{13}$ (MPa)	2437
Shear modulus, G_{23} (MPa)	2855
Poissons ratio, $\nu_{12} = \nu_{13}$	0.298
Poissons ratio, ν_{23}	0.384

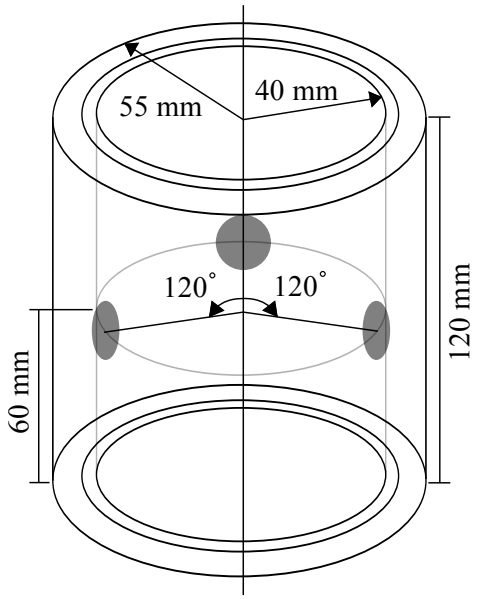

Fig. 2 Test piece geometry and strain gauge rosette positioning

Method

Before testing commenced, each of the pipes was carefully examined for cracks that would prevent use of the data of Table 1 in this analysis. None of the three pipes used in this work contained cracks of any sort and the analytical approach used is therefore valid. The analytical approach to this method also assumes that the removal of layers does not induce residual stresses in the remaining pipe. The layers were consequently removed using a cylindrical grinding machine. It should be mentioned that it is not necessary to remove each ply in a single measuring process. Typically the material removed in each measurement is far smaller than the thickness of the ply. The lead wires of the strain gauges were tucked into the pipe cavity during the grinding process. Grinding forces and heat input were minimised by only taking 0.025 mm off the wall thickness during each pass of the grinding wheel. The use of a thermal imaging camera revealed that the maximum surface temperature that the test pieces reached during machining was in the region of 42°C, as seen in the enclosed area, Ar1, of Fig. 3, which is well below the peak cure temperature of 80°C. Under these conditions it is reasonable to assume that the induced machining stresses are negligible.

To ensure that accurate results were obtained, polynomial curves were fitted to the measured strain data which removed the undue influence of any single datum point. This approach requires that many data points are obtained to provide the necessary redundancy in measurement. For this reason, the strains were measured at every 0.3 mm of removed wall thickness. This required that the test pieces were removed from the grinder and taken to a room in the basement where the temperature was fairly stable. Strain measurements were recorded 4 hours after each layer was removed. The lead wires of the strain gauges were soldered to a National Instruments data acquisition system equipped with SCXI-1520 and SCXI-1521/B strain cards. The time delay allowed the temperature of the test sections and

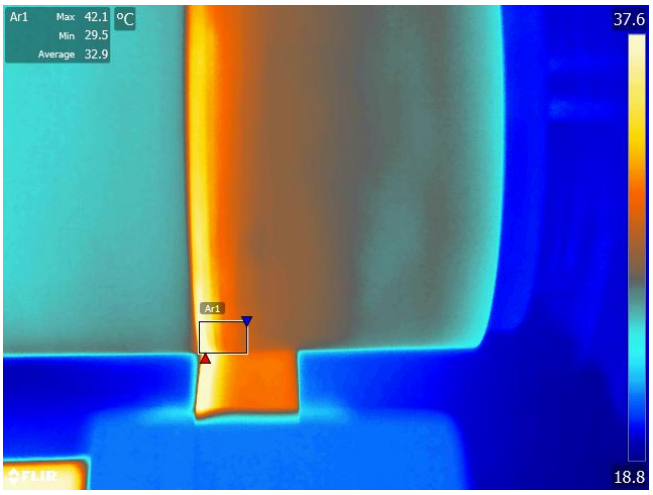

Fig. 3 Thermal image during grinding

the consequent strain measurements to stabilise at the ambient temperature. Due to the time required for each measurement, the entire test took a number of weeks to complete. Over this period, the temperature in the testing environment drifted gradually. For this reason, temperature compensation was used. This was achieved by heating the test environment at every tenth removed layer, and noting the strain response with temperature. From this data, polynomial curves of strain response with temperature over the full cut depth were generated. The measured strain data were then referenced to a single temperature. It was not possible to continue the grinding process beyond about 0.6 mm wall thickness because the test sections became increasingly fragile. The final strain measured for zero wall thickness was consequently obtained by a parting procedure where the wall around the strain gauge rosette was cut through after the strain reading had been recorded for the last layer removal. This effectively released the remaining residual stress, and the final measured strains in each rosette were assumed to be exactly equal and opposite to the residual strains that existed in the inner surface of the pipe prior to any machining process.

Analysis and results

The process of filament winding produces a pipe which is woven in a complex pattern at both the positive and negative values of the desired fibre angle. For this reason, the pipes were assumed to have orthotropic material properties at the bulk scale. The resulting stiffness matrix consequently has no shear coupling terms.

The results measured by the three strain gauge rosettes on each pipe section of a particular layup were found to be very similar. To aid in the clarity of presentation therefore, only the results from a single rosette are shown for each pipe configuration. The measured strain data from one of the rosettes used on the $\pm 55^{\circ}$ test section are illustrated in Fig. 4. A polynomial is fitted to each set of strain data and is used in the calculation of the residual stress distributions. A fifth order polynomial was used for each distribution. Although better fits are possible with higher order polynomials, these curves tend to introduce distinct waviness into the resultant stress distributions. There is no particular reason why such variation should occur and, as a consequence, the order of the polynomial fits was limited to the highest that did not introduce waviness. This approach tends to result in slightly larger error bars than are possible with higher order fits. This is because differences between any measurement and the polynomial fit contribute to the uncertainties surrounding the stress measurements as explained in section 2. Additionally, scatter in individual strain measurements affects the error between the polynomial fit and the measurement. This results in scatter in the magnitude of the error bars. In general, though, the sensitivity of the measurement increases as the wall thickness is progressively removed, and as a consequence, the magnitude of the error bars tends to reduce towards the inner surface of the pipe.

The through-thickness distributions of the axial residual stress, σ_x, and hoop residual stress, σ_θ, and associated error bars, are illustrated in Figs. 5 and 6, respectively. The stresses

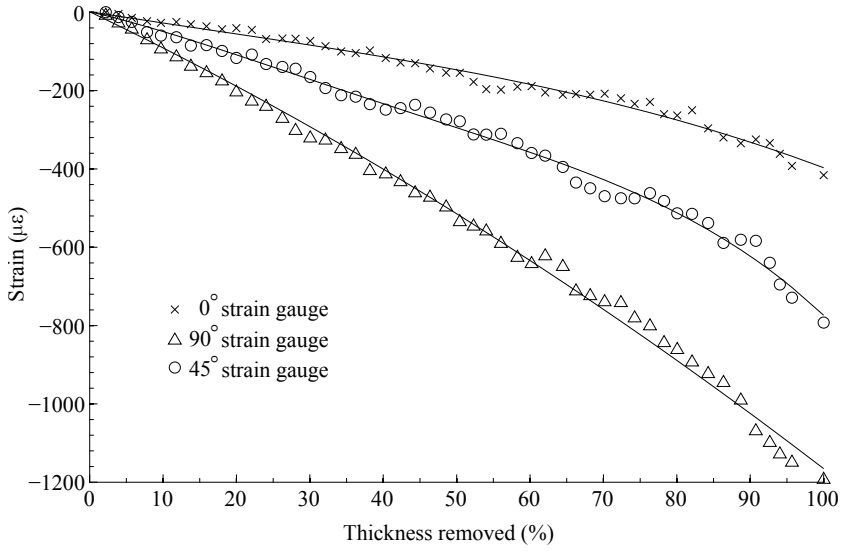

Fig. 4 Measured strain data and polynomial fits for $\pm 55°$ pipe

at the inner surface are represented using the $\times$ symbol. These were calculated under the plain stress assumption, using the values of the polynomials fitted to the strain data. As expected, the axial and hoop stresses of Figs. 5 and 6 are largely linear, with the hoop stress having a larger maximum value than that of the axial stress. Both stress distributions are compressive on the outer walls of the pipe, becoming increasingly tensile toward the inner wall. Extrapolations of the stress distributions to zero wall thickness agree well with the residual stresses at the inner surface of the pipe. Since the value of the inner surface stress is based upon the polynomial fitted to the measured strain distribution, good agreement is expected despite the difference in the procedure for determining these stresses. The axial and hoop stresses were integrated over the wall thickness by assuming that the stress distributions varied linearly between the points on either side of the extrapolation. It was determined that the requirement of self-equilibrium was satisfied within a very small experimental error. The magnitude of the error bars is directly correlated with the quality of the measured strain data. Although great care was taken in ensuring the best possible strain data, the nature of

the material, and the manner of measurement did introduce errors. The error bounds at each measured point are consequently not negligible. The errors associated with the stresses on the inner wall are negligible when compared to the errors associated with the remaining stress distributions since they are only dependent on the difference between the measured strain and the polynomial fit at this position, and do not depend on the errors associated with the preceding data points. This issue is discussed in detail at a later stage in this paper.

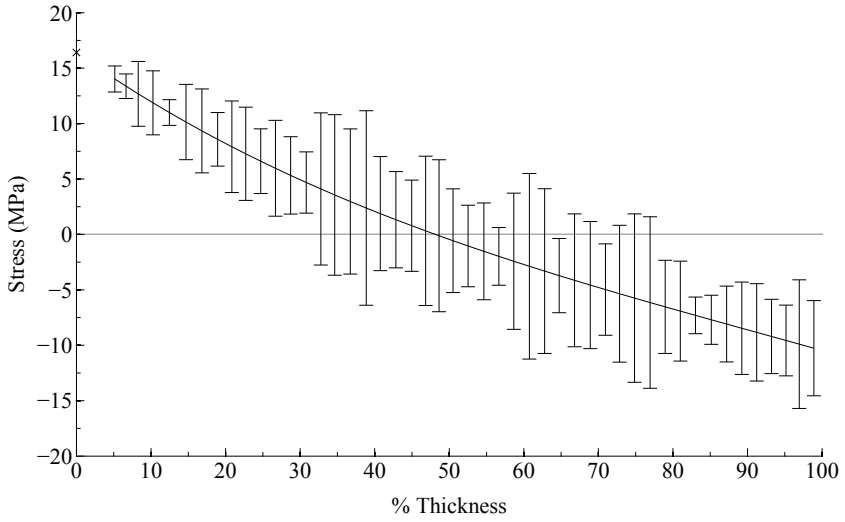

Fig. 5 Axial stress of $\pm 55^\circ$ pipe

The distributions of the radial residual stress, σ_r, and in-plane shear residual stress, $\tau_{x\theta}$, in the $\pm 55^\circ$ test section are presented in Figs 7 and 8, respectively. The radial stress is tensile and, as required, vanishes to zero at the inner and outer surfaces of the pipe. The maximum value of the radial stress is located in the region of 40% through the pipe thickness and is about an order of magnitude smaller than those of the axial and hoop stresses. The errors in the radial stress, however, are not significantly affected by the quality of the measured strain data. The shear stress distribution in Fig. 8 remains very close to zero as required by the

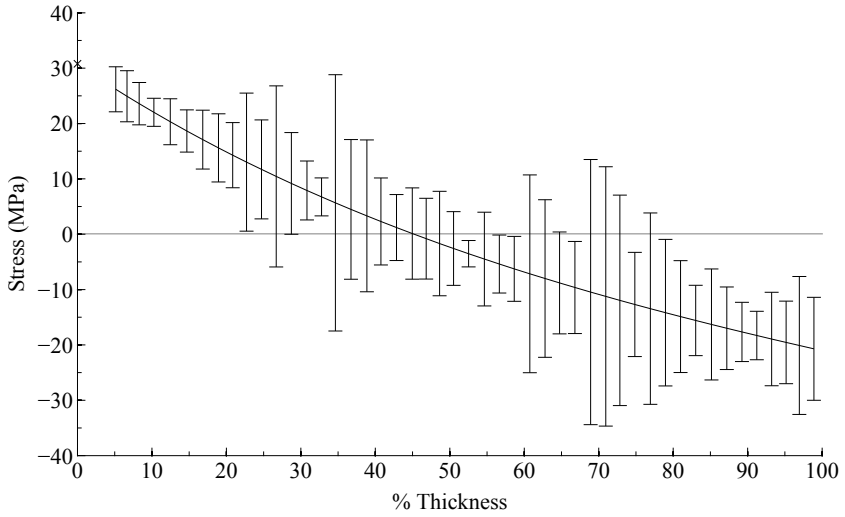

Fig. 6 Hoop stress of $\pm 55^\circ$ pipe

orthotropic layup of the pipe. The error bars are fairly large because of the complex weave and stacking of the plies at both $+55^\circ$ and -55°. Any particular layer removed over a selected strain gauge rosette almost certainly involves the removal of more material orientated in a particular direction than the other which results in a measurable shear strain response. It is clear from Fig. 4 that a distinct waviness in the shear strains exists as a consequence of spatial aliasing arising from the thickness of each layer removed versus the distance over with which the weave pattern repeats. This waviness is the source of the large error bars.

The measured strain data from one of the rosettes of the layered pipe with fibre directions of $\pm 75^\circ$ and $\pm 36^\circ$ in the inner and outer parts of the wall, respectively, are presented in Fig. 9 with the corresponding least squares polynomial fits. The polynomial least squares fits have discontinuous slopes at the interfaces between the two fibre directions as is required because of the change in material properties. The polynomial fits for the outer $\pm 36^\circ$ section are of fifth order, and the polynomial fits for the inner $\pm 75^\circ$ section are of second order, except for the 0° strain gauge, for which the fit is third order.

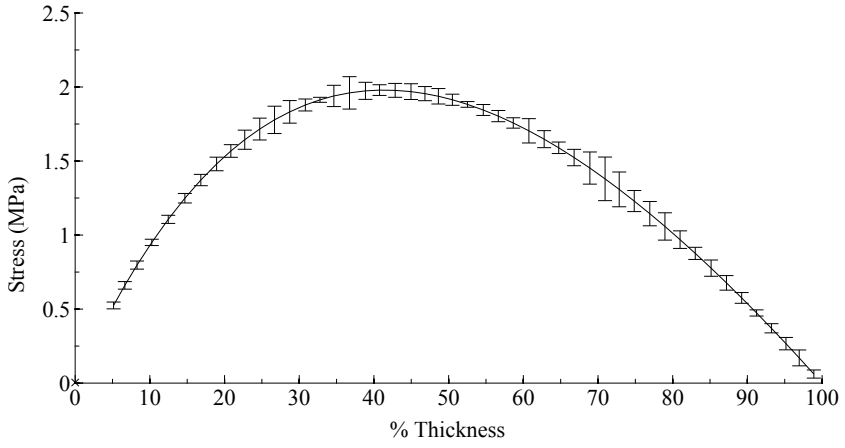

Fig. 7 Radial stress of $\pm 55°$ pipe

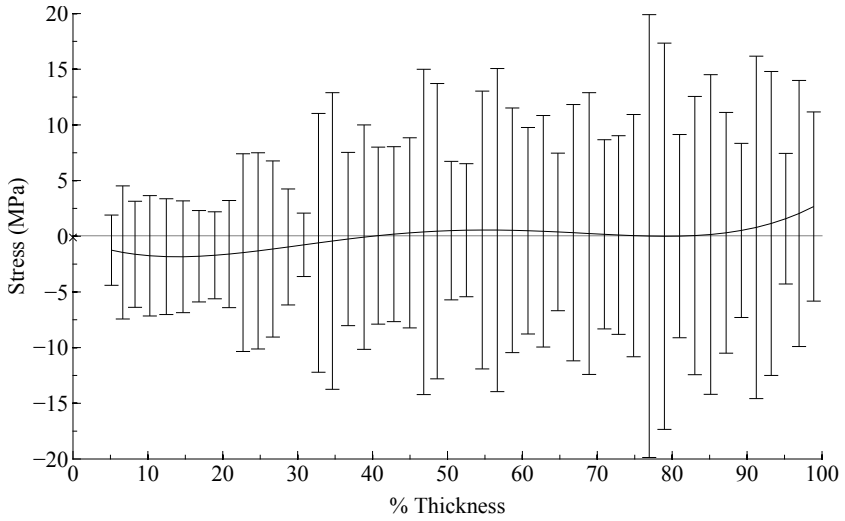

Fig. 8 Shear stress of $\pm 55°$ pipe

Figs. 10 and 11 present the residual stress distributions in the axial and hoop directions, σ_x and σ_θ respectively, corresponding to the strain variations of Fig. 9. As was the case for the $\pm 55°$ pipe, extrapolations of both the axial and hoop stress distributions to zero wall thickness are in close agreement with the stresses calculated assuming a state of plain stress applied to the polynomial fit at the inner wall. Both stresses also satisfy the self-equilibrium

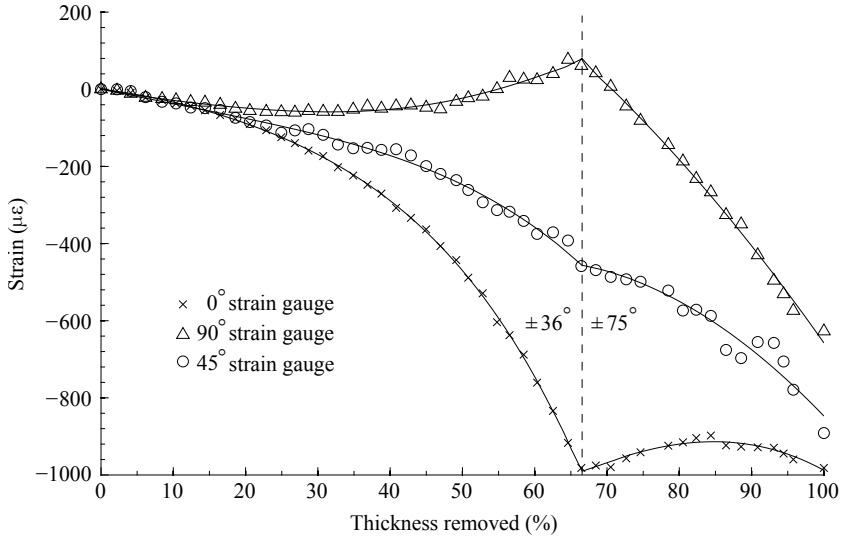

Fig. 9 Measured strain data and polynomial fits for ±75°/±36° layered pipe

requirement. It is also evident that the stress distributions are discontinuous at the interface between the ±75° and ±36° sections. Such discontinuities are expected as a consequence of the change in elastic stiffness. The discontinuities in the hoop stress of Fig. 11 are, however, different from what is expected. The stress in the outer ±36° section is tensile, while the stress of the ±75° section is compressive. It is expected that both stresses have the same sense and that the magnitude of the hoop stress in the ±75° section is higher due to the greater stiffness of the material in this direction. The fact that the stresses have an opposite sense indicates that the residual strains are discontinuous between the two layers. This somewhat unexpected result can be explained by considering the method by which the pipe was manufactured. The pipe was laid up in two stages with two cure cycles. The first cure cycle was performed after the ±75° fibres had been wound and the second was performed after the ±36° fibres had subsequently been wound. This two-stage manufacturing process introduces residual stresses separately into each pipe section at each stage and significantly reduces the likelihood of the residual strains matching at the ply interface. It is apparent from

Figs. 10 and 11 that the two-stage manufacturing process results in the formation of residual axial and hoop stresses that are very similar at the inner surface to those of the $\pm 55^\circ$ pipe of Figs. 5 and 6. This is an interesting result, considering the very different stiffnesses in the principal directions as a consequence of the different winding angles of the pipe sections. The impact of the two-stage manufacturing process on the residual stresses is further evident when the general nature of the curves of Fig. 11 is considered. Both the inner and outer sections of the pipe follow the trend evident in Fig. 6 which shows the hoop stress of the $\pm 55^\circ$ pipe. This indicates that each section of the layered pipe generated internal residual stresses as it was cured, without significant interaction between the two sections.

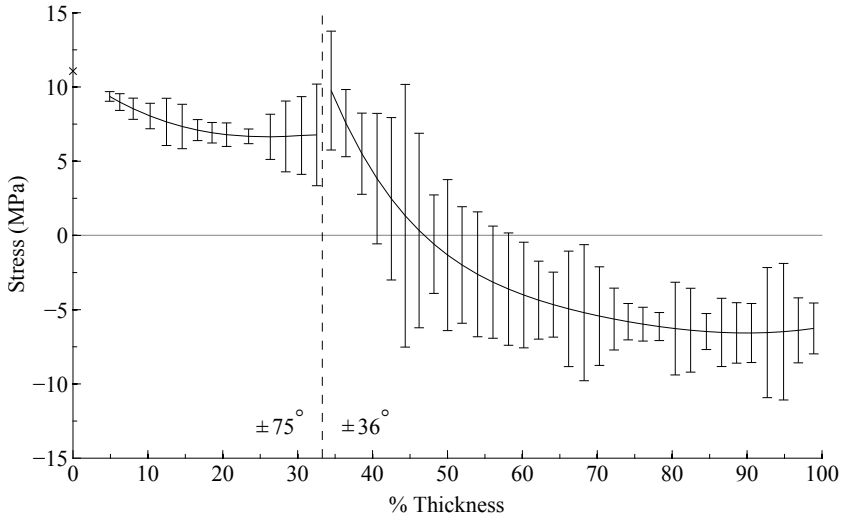

Fig. 10 Axial stress of $\pm 75^\circ/\pm 36^\circ$ layered pipe

This hypothesis is confirmed when the radial residual stress, σ_r, presented in Fig. 12, is examined. It is clear that the stress distribution has two distinct peaks, each near the mean radius of the corresponding section of the pipe. Each of the peaks results from the development of residual stresses in that section. Although the interaction between the two

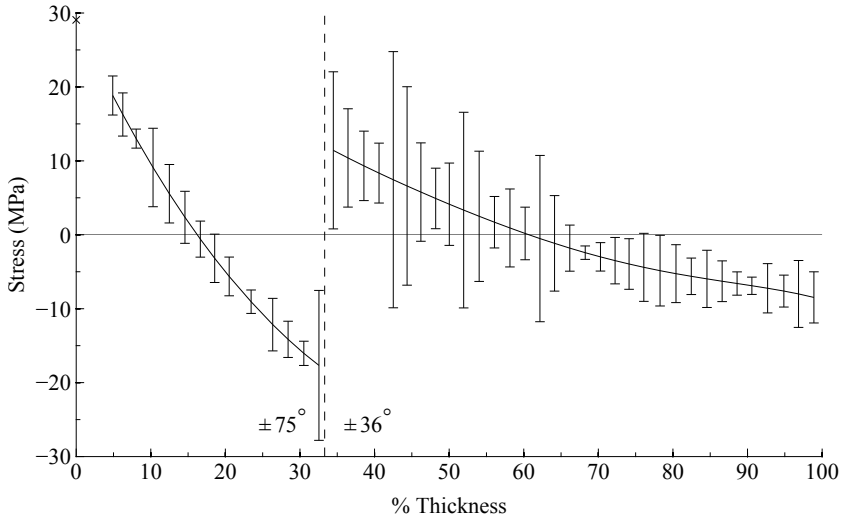

Fig. 11 Hoop stress of ±75°/±36° layered pipe

sections is not significant, some interaction is evident because the radial residual stress is about 0.15 MPa at the interface. Without any interaction, this stress would be zero. In comparison to the ±55° pipe, the errors in radial stress seem somewhat larger, but this is only because the radial stress distribution of Fig. 12 is smaller than that of Fig. 7.

The distribution of the in-plane shear stress, $\tau_{x\theta}$, in Fig. 13 oscillates around zero stress throughout the thickness. As with the ±55° pipe, the shear stress distribution is expected to be zero as a consequence of the bulk-scale orthotropy. At a finer scale though, stacking of alternating plies produces significant alternating shear stresses, and consequent oscillations in the measured shear strain distribution. These oscillations are the source of the large error bounds in the shear stress distribution.

The measured strain data from one of the rosettes of the ±65°/±47° layered pipe are presented in Fig. 14 with the corresponding least squares polynomial fits. As with the strain data of Fig. 9, the polynomials have a discontinuous slope at the region of the layer interface as a consequence of the differences in material properties of the ±65° and ±47° layers. The

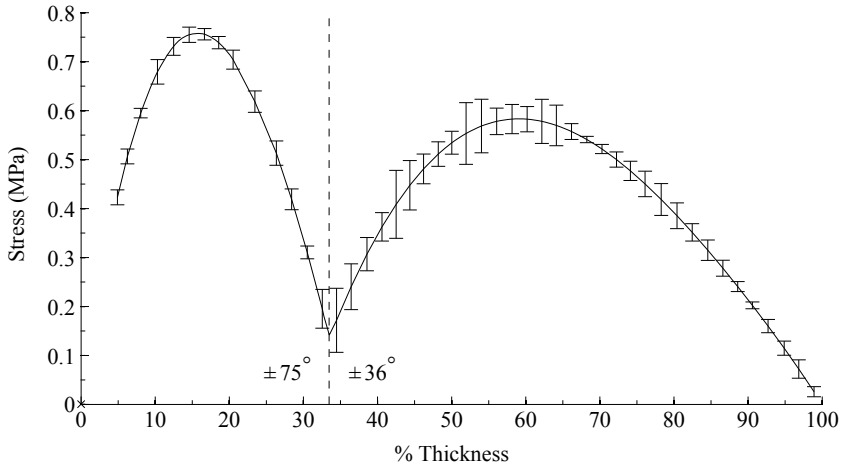

Fig. 12 Radial stress of ±75°/±36° layered pipe

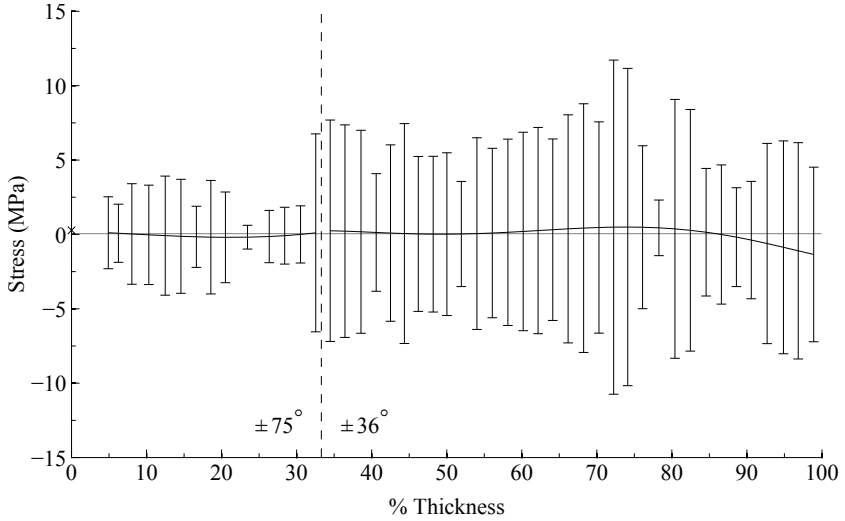

Fig. 13 Shear stress of ±75°/±36° layered pipe

polynomial fits corresponding to the removal of the outer ±47° section are fifth order, while the the polynomial fits corresponding the the removal of the inner ±65° section are limited to second order. Although the polynomials fit the data well, there is some scatter, especially for the 45° strain gauge.

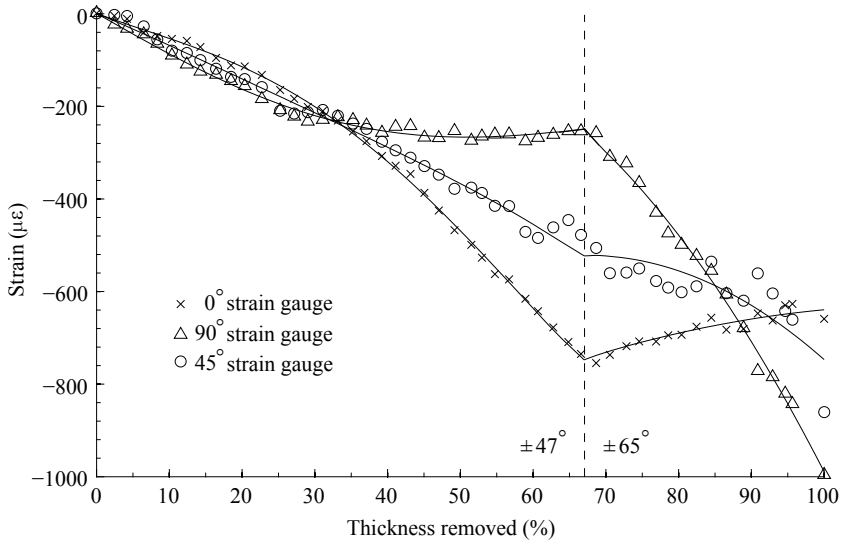

Fig. 14 Measured strain data and polynomial fits for ±65°/±47° layered pipe

The residual axial stress, σ_x, and hoop stress, σ_θ, are presented in Figs. 15 and 16, respectively. Both stress distributions are fairly linear in the outer region of the pipe, which is wound at ±47°. In this respect, the results are slightly unexpected since it would be anticipated that the stress distributions in this region would fall between those of the ±55° pipe and that of the ±75°/±36° pipe. The axial stress distribution in the outer section of the latter pipe is distinctly non-linear and so the near-linear variation of this stress in the ±65°/±47° pipe is a bit unexpected. This might be explained by considering that a fairly linear distribution would be expected for a single winding angle. In the case of the ±65°/±47° pipe, the axial material properties in the two layers are more similar that those of the ±75°/±36° pipe and so the resultant stress distribution would be expected to be far more similar to the fairly linear distribution of the ±55° pipe than the non-linear distribution of the ±75°/±36° pipe. In contrast to the axial stress, the hoop stress distribution has, however, a form similar to that anticipated and represents a strain discontinuity at the ply interface. Both the axial and hoop stresses, like those of the ±55° and ±75°/±36° pipes, satisfy the self-equilibrium require-

ment. Interestingly, the axial and hoop residual stresses at both the inner and outer surfaces of the layered pipe are comparable to those of the ±55° pipe presented in Figs. 5 and 6, despite the significant difference in stiffnesses in the principal directions of the respective pipe sections.

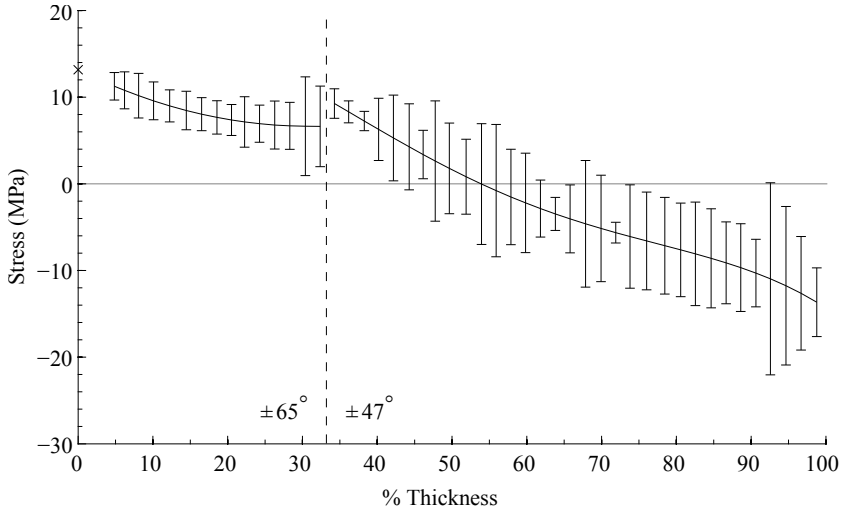

Fig. 15 Axial stress of ±65°/±47° layered pipe

The residual radial, σ_r, and in-plane shear stresses, $\tau_{x\theta}$, are presented in Figs. 17 and 18. Both of these distributions conform with expectations. The twin peaks of the radial stress are far less pronounced than those evident in Fig. 12 and the stress distribution is tending back to the single peak of the ±55° pipe presented in Fig. 7. The in-plane shear stresses are small with fairly significant error bars, the reason for which has already been explained. An extrapolation of the shear stress to zero wall thickness once again satisfies the self-equilibrium requirement.

One may have noticed that the error bars for the stress components on the inner surface of all pipes were not shown. This is because they were very small in comparison to the

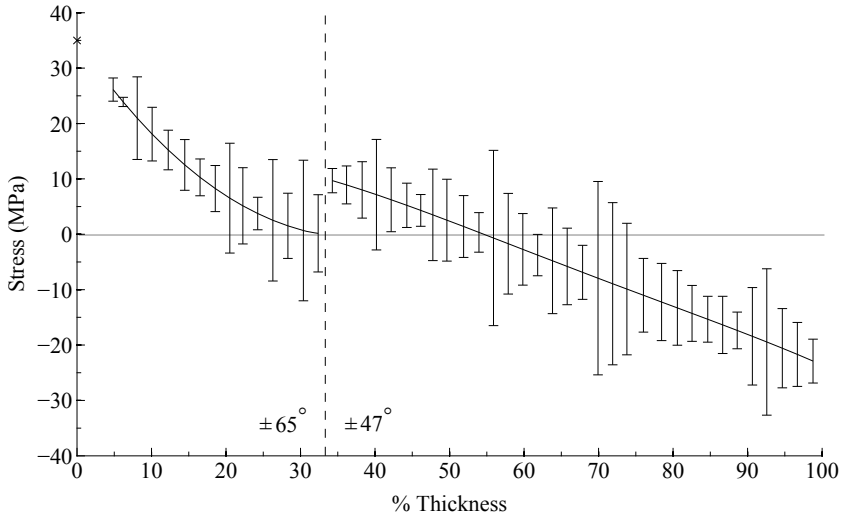

Fig. 16 Hoop stress of ±65°/±47° layered pipe

error bars elsewhere through the thickness. This is a consequence of the error depending only on the difference in least-fit strain and measured strain at this position, and not on any preceding measurements. To illustrate this, the 45° strain gauge of Fig. 14 is considered. The difference between the polynomial fit and measured value is about $100\mu\varepsilon$. This corresponds to an error, for instance, in shear stress of 0.76 MPa, which is very small in comparison to the error bars displayed in Fig. 13.

4 Conclusions

The residual stress distributions in three thick-walled GFRP filament-wound pipe sections of 80 mm inner diameter and 15 mm wall thickness were measured using the layer removal method proposed by Carpenter et al. [24]. The first of the pipes was the industry standard of ±55° with a single cure cycle. The remaining pipes were layered sections with ±75°/±36° and ±65°/±47° combinations, each manufactured with a two-stage cure procedure. It was found that the order of the least-squares polynomial that was fitted to each mea-

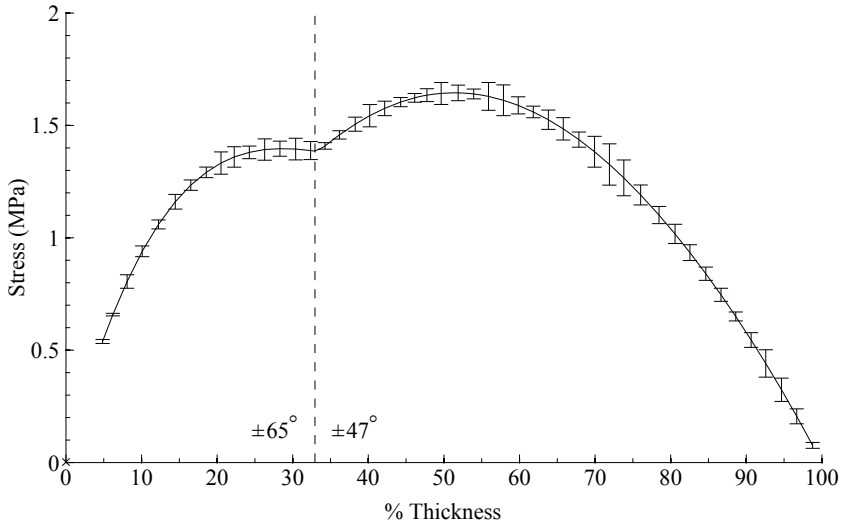

Fig. 17 Radial stress of ±65°/±47° layered pipe

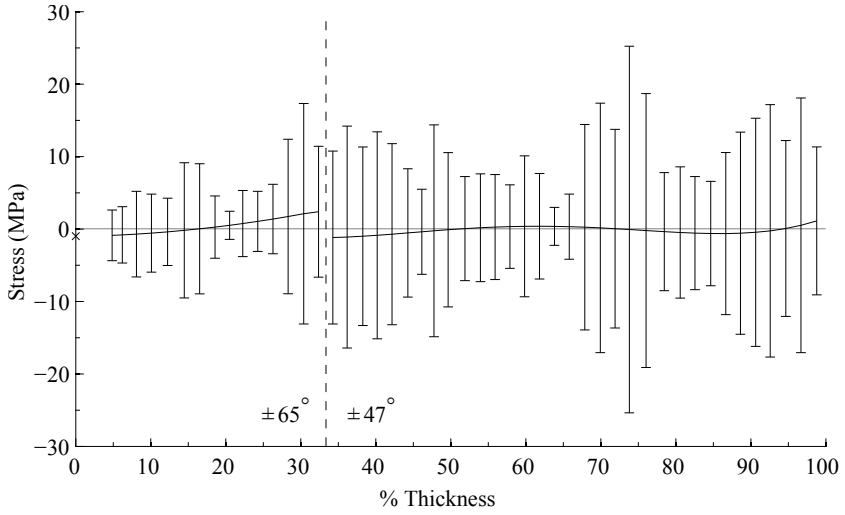

Fig. 18 Shear stress of ±65°/±47° layered pipe

sured data set needed to be limited to minimise waviness in the resulting stress distributions. Due to the pipe becoming increasingly fragile when very thin, the residual strain distributions could not be measured near the inner surface. A method of parting was consequently used to obtain the inherent residual strain, and thus the residual stress, on the inner surface

of each of the pipes. Extrapolations to the inner wall of the stress distributions obtained using the layer removal process are in close agreement with the residual stresses measured there using the parting method. The extrapolated axial, hoop and shear stress distributions adhere to the requirement of self-equilibrium. In addition, the radial stress distributions all vanish to zero at the inner and outer surfaces, as required. The resulting axial and hoop stresses at the inner surfaces of both the layered pipes were similar in magnitude and sense to the $\pm 55^\circ$ pipe section. The axial and hoop stresses obtained for the $\pm 65^\circ/\pm 47^\circ$ pipe at the outer surface were also similar to those measured for the $\pm 55^\circ$ pipe section. It was found that the residual strains at the interface of each of the layered pipes were discontinuous, a consequence of the two-stage manufacturing procedure of these pipes. This suggests that two separate stages of residual stress development occurred, which is evident also in the tendency of the radial stresses of the layered pipes to have two distinct peaks, one for each layer.

Acknowledgements

The support of the DST/NRF Centre of Excellence in Strong Materials (CoE-SM) towards this research is hereby acknowledged. Opinions expressed and conclusions arrived at, are those of the authors and are not necessarily to be attributed to the CoE-SM.

References

1. Yu.M. Tarnopol'skii, G.G. Portnov, and Yu.B. Spridzans. Compensation of thermal stresses in glass-fiber-reinforced plastic articles by the layerwise winding method. *Polymer Mechanics*, 8(4):553–557, 1972.

2. H. Gong, Y. Wu, and K. Liao. Research on residual stress measurement technology of aluminum alloy plate based on modified layer removal method. In *1st International Conference on Information Science and Engineering, ICISE*, pages 3839–3842, 2009.
3. F. Yang, Y. Wang, and J. Jiang. Residual stress profile in high carbon rods measured by layer removal technique. *Cailiao Kexue yu Gongyi/Material Science and Technology*, 18(4):579–583, 2010.
4. W. Cheng and I. Finnie. *Residual Stress Measurement and the Slitting Method*. Springer, 2007.
5. M. B. Prime. Residual stress measurement by successive extension of a slot: The crack compliance method. *Applied Mechanics Reviews*, 52(2):75–96, 1999.
6. M. B. Prime. Measuring residual stress and the resulting stress intensity factor in compact tension specimens. *Fatigue and Fracture of Engineering Materials and Structures*, 22(3):195–204, 1999.
7. M. B. Prime and M. R. Hill. Measurement of fiber-scale residual stress variation in a metal-matrix composite. *Journal of Composite Materials*, 38(23):2079–2095, 2004.
8. A. T. DeWald and M. R. Hill. Measurement of bulk residual stress distributions in thick-section components using the contour method. In *Conference Proceedings of the Society for Experimental Mechanics Series*, volume 8, pages 29–31, 2011.
9. P. Pagliaro, M. B. Prime, H. Swenson, and B. Zuccarello. Measuring multiple residual-stress components using the Contour method and multiple cuts. *Experimental Mechanics*, 50(2):187–194, 2010.
10. M. T. Flaman and B. H. Manning. Determination of residual-stress variation with depth by the hole-drilling method. *Experimental Mechanics*, 25(3):205–207, 1985.
11. O. Sicot, X. L. Gong, A. Cherouat, and J. Lu. Influence of experimental parameters on determination of residual stress using the incremental hole-drilling method. *Composites Science and Technology*, 64(2):171–180, 2004.
12. G. Sachs. The Determination of Residual Stresses in Rods and Tubes. *Zeitschrift für Metallkinde*, 19:352–357, 1927.
13. A. Stacey and G. A. Webster. Determination of residual stress distributions in autofrettaged tubing. *International Journal of Pressure Vessels and Piping*, 31(3):205–220, 1988.
14. J. W. Kim and D. G. Lee. Measurement of residual stresses in thick composite cylinders by the radial-cut-cylinder-bending method. *Composite Structures*, 77(4):444–456, 2007.
15. M. A. Seif and S. R. Short. Determination of residual stresses in thin-walled composite cylinders. *Experimental Techniques*, 26(2):43–46, 2002.

16. M. A. Seif, U. A. Khashaba, and R. Rojas-oviedo. Residual stress measurements in CFRE and GFRE composite missile shells. *Composite Structures*, 79(2):261–269, 2007.

17. S. Akbari, F. Taheri-Behrooz, and M. M. Shokrieh. Slitting Measurement of Residual Hoop Stresses Through the Wall-Thickness of a Filament Wound Composite Ring. *Experimental Mechanics*, pages 1–10, 2013.

18. B. M. Botros. Residual stresses in cold ironed tubes. *International Journal of Mechanical Sciences*, 2(3):195–205, 1960.

19. D. R. Mack. Measurement of residual stress in disks from turbine-rotor forgings - Investigation reveals that both the sachs turning-down method and the concentric-ring method provide reliable measurements of tangential residual stress in a steel disk at the bore hole. *Experimental Mechanics*, 2(5):155–158, 1962.

20. J. Chen, T. Terasaki, T. Akiyama, and K. Kishitake. New concept of equivalent inherent strain for measuring axisymmetric residual stresses. *Journal of Manufacturing Science and Engineering, Transactions of the ASME*, 122(2):304–309, 2000.

21. W. A. Olson and C. W. Bert. Analysis of residual stresses in bars and tubes of cylindrically orthotropic materials - Paper presents equations for calculating residual stresses from surface-strain data measured after successive borings in a bar or tube made of a cylindrically orthotropic material. *Experimental Mechanics*, 6(9):451–457, 1966.

22. G. Z. Voyiadjis, P. D. Kiousis, and C. S. Hartley. Analysis of residual stresses in cylindrically anisotropic materials. *Experimental Mechanics*, 25(2):145–147, 1985.

23. G. Z. Voyiadjis and C. S. Hartley. Residual-stress determination of concentric layers of cylindrically orthotropic materials. *Experimental Mechanics*, 27(3):290–297, 1987.

24. H.W. Carpenter, R.G. Reid, and R. Paskaramoorthy. Extension of the layer removal technique for the measurement of residual stresses in layered anisotropic cylinders. *International Journal of Mechanics and Materials in Design*, pages 1–12, 2014.

25. C. T. Herakovich. *Mechanics of Fibrous Composites*. John Wiley & Sons, Inc., 1998.

26. J. P. Holman. *Experimental Methods for Engineers*. McGraw-Hill, eighth edition, 2012.

27. M. B. Prime and M. R. Hill. Uncertainty analysis, model error, and order selection for series-expanded, residual stress inverse solutions. *Journal of Engineering Materials and Technology*, 128(2):175–185, 2006.

28. ASM International. *Engineered Materials Handbook - Desk Edition*. Materials Park, Ohio, 1995.